Journal of Materials Research and Technology 33 (2024) 2210–2215

Contents lists available at ScienceDirect

Journal of Materials Research and Technology

journal homepage: www.elsevier.com/locate/jmrt

Reliability of the Young's modulus of crab exoskeleton materials estimated from nanoindentation tests

Tadanobu Inoue *, Qiu Hai, Koji Nakazato

National Institute for Materials Science, 1-2-1, Sengen, Tsukuba, 305-0047, Japan

ARTICLE INFO

Handling editor: P.Y. Chen

Keywords:
Biomaterials
Mechanical properties mapping
Crustacean material
Nanoindentation
Tension test

ABSTRACT

The local and global mechanical properties of a mineralized biological material using the mud crab as a model material were investigated and compared. The stress–strain (s–s) curves for wet and dry conditions of the endocuticle were exactly examined by performing tensile tests with strain gauges. The local properties were examined through nanoindentation testing (NI) in a dry condition. The global Young's modulus, *E*, evaluated from the slope of the linear part of the s–s curve, did not vary with wet or dry specimen conditions; however, the stress and strain required to fracture depended on the conditions. The *E* was compared with the results of property mapping obtained from NI. Due to local differences in the grade of mineralization in the exoskeleton, the mapping indicated that nanoindentation tests should be performed for an extensive region of the cuticle. The results will provide useful information for future material development based on biomimetics.

1. Introduction

Research into the complex tissue structures of organisms is often carried out as a technique for breaking through the characteristic limits of materials [1–4] . For example, a twisted–plywood pattern structure (TPS) is observed in the robust exoskeleton of arthropods, and the superior properties of the TPS and its mechanism have been studied [5–8]. However, the exoskeleton of organisms is wholly gently curved [9] and is thin and small compared to the sample size for the mechanical testing of ordinary metallic materials; furthermore, the mechanical properties of the exoskeleton strongly depend on the sample condition—wet or dry [10–14]. In most studies, the local mechanical properties of the exoskeleton in a dry condition have been evaluated by a nanoindentation (NI) test or Vickers hardness test, and the relationship between the microstructure and local properties (hardness, stiffness, wear resistance) is examined [7,8,10,15]. In particular, there has been remarkable progress in recent research into NI [16–18]. On the other hand, in some studies, to investigate the properties of the exoskeleton as a bulk sample, a small sample was extracted from the exoskeleton, and tensile or bending tests were performed under wet and dry conditions [10–14]. However, there are few studies that have used strain gauges to accurately investigate the stress–strain response, which is directly linked to the Young's modulus. Since the exoskeleton is a composite structure composed of the epi-, exo-, and endocuticles and membranous [5,7, 10–12,14,15,19,20], the sample must be extract from each layer by machining. Furthermore, inside the exoskeleton, there are thick pore canal tubes (pcts) perpendicular to the surface, thin pcts in two directions normal to it, and numerous pore canals (pcs) in the mineralized matrix [4,7,10,12,19,20]. Their tubes and pores should act as initial defects in the test sample and significantly affect the stiffness in the mechanical properties. In biomaterials, the properties of the sample change with elapsed time. NI tests are usually performed under dry conditions after 48 h or more of sample preparation, including the curing time of the embedded resin. In biological materials, there is a high possibility that the local properties obtained from the NI test under this condition will not always agree with the data of the organism's bulk properties.

In this paper, the claw of the mud crab, *Scylla serrata*, which has a relatively large body among crustaceans, was selected for the exoskeleton sample. We attempted to compare the NI test with a highly reliable tensile test method using a strain gauge for Young's modulus.

2. Materials and methods

Two very large mud crabs in the intermolt stage were obtained live from a local market in Naha, Okinawa, Japan. These crabs were the largest crabs in the market. The body weight (*BW*) of the sample male crabs was 2138 g (right claw: samples A; left claw: sample B) and 2038 g

* Corresponding author.
E-mail address: INOUE.Tadanobu@nims.go.jp (T. Inoue).

https://doi.org/10.1016/j.jmrt.2024.09.194
Received 18 August 2024; Received in revised form 10 September 2024; Accepted 23 September 2024
Available online 25 September 2024

(left claw: sample C).

After deep-freezing, the mud crab was transported to NIMS in Tsukuba. After thawing under running water (Fig. 1(a)), the size of each part was measured with vernier calipers. After that, specimens for tensile testing were immediately cut from each claw with a high-performance precision micro grinder (MINITOR Co.,Ltd., Minimo ONE SERIES Ver.2, Tokyo, Japan) with diamond cutting discs (Fig. 1(b)). Since the crab claws are gently curved as a whole, tensile specimens were taken from relatively parallel region of the claws. On the mud crab of 2138 g, 16 rectangular specimens approximately 23–25 mm in length by 9–11 mm in width were cut from the right (sample A) and left claws (sample B), and 10 rectangular specimens on the mud crab of 2038 g shown in Fig. 1(a and b) were cut from the left claw (sample C). Details of the specimen preparation procedure are shown in Fig. S1 of the supplementary material. First, the test specimens were processed into 22 × 8 mm rectangles using a micro grinder (*Step* 1). The top and bottom of the specimen were ground with a grit 320 grade silicon carbide (SiC) paper to obtain a specimen consisting only of the endocuticle layer, which is thickest in the exoskeleton (*Step* 2). Subsequently, to make a dumbbell specimen, rectangular specimens were ground into a roughly dumbbell shape with a micro grinder with abrasive rubber points (*Step* 3). Next, these specimens were finished as a dumbbell specimen to a size of 6 mm in gauge length (GL) and 2 mm in width using SiC paper. Finally, they were ground with grit 320/600/800/1200 grade SiC papers to minimize the effect of the specimen edges on tensile testing (Fig. 1(c), *Step* 4). The surface variation of the width edges of the specimen against a grade of SiC paper is shown in Fig. S2 of the supplementary material. For each sample, after the rectangular specimens were cut out, all specimens were kept in pure water to prevent desiccation during preparation, except during polishing and grinding. For each sample A, B, and C, specimen preparation began at 9:00 a.m. and ended at 3:00 p.m. All specimens were then taken to the laboratory for tensile testing while kept in pure water.

Tensile tests, with a crosshead speed of 1 mm/min, were conducted at 23 °C [21,22] on 15 specimens (wet condition) immediately after specimen preparation and on 11 specimens (dry condition) 24 h after specimen preparation (Fig. 1(d)). Strain gauges 0.84 mm in width and 2 mm in length (KFGS-2N-120-C1-11 L50C2R, KYOWA Co., Ltd., Tokyo, Japan) were attached to both the top and bottom of each specimen. The nominal strain, ε, was presented as the average of the data measured with two strain gages. The Young's modulus, E, was evaluated from the slope of the linear part of the stress(σ)−ε curve. The fracture surface after testing was observed through a 3D laser scanning microscope (VK-X200/210, Keyence Corporation, Osaka, Japan).

NI testing was performed using nanoindentation equipment with a Berkovich-type diamond indenter with an angle of 115° (ENT-NEXUS, ELIONIX, Tokyo, Japan). To perform it, the sample was taken from the GL region of the BT9 dry specimen after a tensile test on sample C (Fig. 1(e)), and it was embedded in epoxy and polished. Details of the procedures for the treatment of the specimen surfaces were given earlier [7,23,24]. First, the cross-sectional tissue before the NI test was observed with a 3D laser scanning microscope. In the NI test, the loading curve consisted of a 5 s loading to 5 mN, followed by a 5 s hold at that force, and then a 5 s unloading. The first indentation made in the cross section was placed at least 10 μm away from the edge, and successive indentations were made every 50 μm until the end was reached. The hardness (H_{IT}) and reduced elastic modulus (E_r) were analyzed from the unloading curve by using the Oliver–Pharr method employed in biological studies [7,8,15,25,26]. The Young's modulus (E_S) of the sample was described by

$$E_S = \frac{1-\nu_S{}^2}{(1/E_r)-(1-\nu_I{}^2)/E_I}, \tag{1}$$

where ν_s and ν_I are Poisson's ratios of the sample and indenter tip, respectively. In the nanoindentation tests, $E_I = 1140$ GPa and $\nu_I = 0.07$

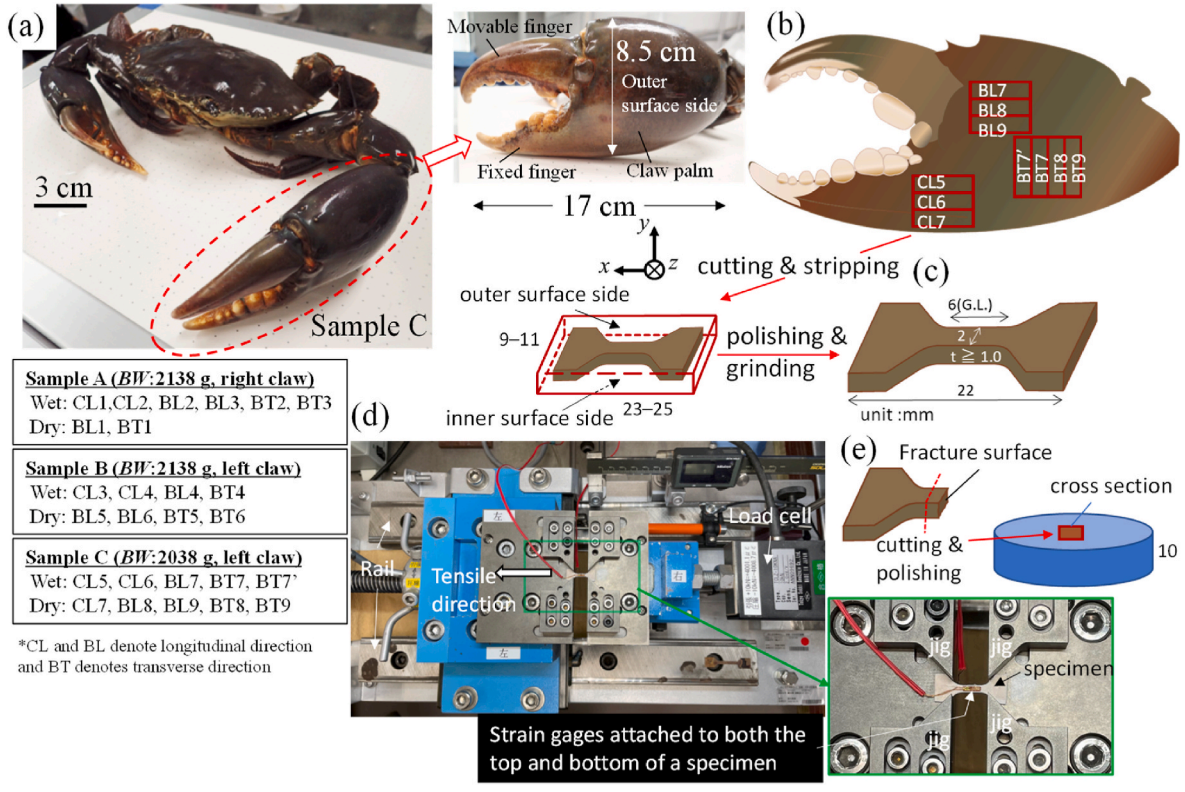

Fig. 1. (a) The mud crab with a body weight (*BW*) of 2038 g and the left claw used as sample C, (b) procedure for preparing tensile test pieces from the claw (sample C), (c) dumbbell specimens, (d) measurement system of the tensile test used, and (e) sample of nanoindentation test and fracture surfaces after tensile testing. The table represents the relationship between test conditions and number of pieces for each sample.

were used for the diamond tip, and $\nu_s = 0.30$ for sample [27]. The contour maps of H_{IT} and E_S were created using SigmaPlot 14.5 (HULINKS Inc., Tokyo, Japan). After NI testing, to verify the distribution of mineralization in the sample, energy-dispersive X-ray spectroscopy (EDS) attached to a focused ion beam –a scanning electron microscope dual-beam instrument (Scios 2, Thermo Fisher Scientific, Waltham, Massachusetts, USA) was used at an accelerating voltage of 15 kV. Before analysis, the sample was coated with about 2 nm of osmium (Neo Osmium Coater, Meiwafosis Co., Ltd., Tokyo, Japan) [7,19,21,24,26].

3. Results and discussion

Fig. 2 show the $\sigma-\varepsilon$ curves for all samples. The $\sigma-\varepsilon$ curves for 6 specimens (BL3, CL3, CL4, CL6, BT7, BT7′) of 14 specimens in the wet condition were a non-linear, while all specimens in the dry condition broke in a linear relationship. Table 1 summarizes the mechanical properties (Young's modulus, E; fracture stress, σ_f; strain to fracture, ε_f) of 26 tests of samples taken from three claws. There was no clear difference in the specimen positions in claws and direction (longitudinal (CL, BL) and transverse (BT)), but there was a difference in the specimen conditions. The wet specimen σ_f ranges from 22.7 to 50.5 MPa, and the average σ_f—including their standard deviation—is 35.0 ± 9.37 MPa at an average ε_f of 0.28 ± 0.08%. The dry specimens have $12.3 \leq \sigma_f \leq 38.1$ MPa and break at $\sigma_f = 28.9 \pm 7.62$ MPa at an average ε_f of 0.22 ± 0.06%. Therefore, the average σ_f and ε_f for the wet condition were higher than those for the dry condition. This is consistent with the previous results reported in tensile testing of the mud crab [13], the American lobster, *Homarus americanus* [12], and the sheep crab, *Loxorhynchus grandis* [10]. On the other hand, the E, for the wet specimens ranged from 10.2 to 17.4 GPa, with an average value of $E = 13.2 \pm 1.71$ GPa, whereas it was $11.8 \leq E \leq 16.2$ GPa and $E = 13.3 \pm 1.17$ GPa for the dry specimens. That is, the E did not depend on the specimen condition. In tensile and bend tests of the endocuticle and the exocuticle of crustaceans reported so far, the E was larger under the dry condition than under the wet condition [10–14]. In general, the E depends on the major components of the material and the texture of the microstructure. That is, the E should be different from the mechanical properties of pcts and chitin–protein bundles that change with the presence of water, such as σ_f and ε_f. Rather, this result—that the E of organisms does not depend on the specimen condition—is reasonable. In past studies [10–13], strain gauges were not used in tension testing, so the E is one order of magnitude smaller than that in the present results, despite using the exoskeleton of the same crustacean, and their strains to fracture are also much larger than the present ε_f.

Fig. 3 shows four specimens after tensile tests and fracture surfaces. Striation patterns originating from the TPS consisting of the endocuticle [12,20,23,24] were observed on all fracture surfaces. In the wet condition, the trace of pct//x (red arrows) observed on the fracture surfaces of BL7 was not observed on the fracture surface of CL6, which showed nonlinear behavior in the $\sigma-\varepsilon$ curves (Fig. 2(e)). Such a trace of pct//x was observed in BL9 for the dry specimen fractured at low stress, but not in the BT9 dry specimen. In the previous paper on mud crabs [24], we reported that there was a large tube that bundled many pcts that penetrated the exoskeleton, and that this tube was thick (62–66 μm) near the inner side and narrowed (12–22 μm) toward the outer surface. Longitudinal streaks observed on the BL9 fracture surface correspond to these large tubes. In the 24 tensile tests conducted in the present study, GL fracture occurred in 10 specimens, and outside GL fracture occurred in 14 specimens. This is due to the presence of pct//x and the distribution of mineralization in the endocuticle sample rather than the accuracy of test specimen preparation. Natural defects, such as a thick tube penetrating the exoskeleton, are large enough to affect the fracture

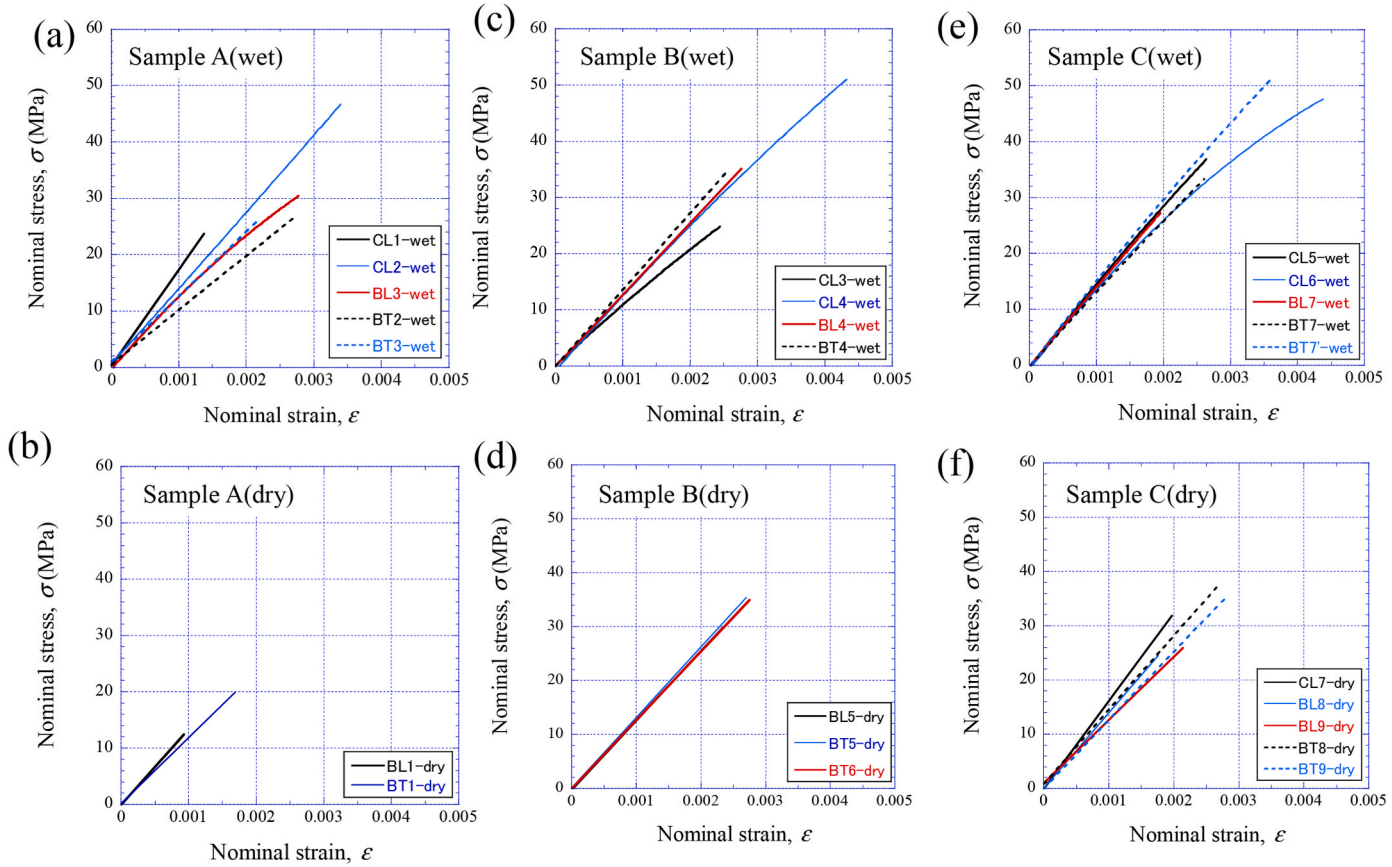

Fig. 2. Nominal stress – nominal strain curves of wet and dry conditions for samples A, B, and C: (a) sample A(wet); (b) sample A(dry); (c) sample B(wet); (d) sample B(dry); (e) sample C(wet); and (f) sample C(dry).

Table 1
Specimen conditions (wet/dry) and results of tensile testing. Here, t and w are thickness and width in gauge length of the dumbbell specimens measured before test, respectively. The Young's modulus, E, was evaluated from the slope of the linear part of the stress-strain curve.

Mud crabs	Specimen positions in claws	No.	Gauge length (GL)		specimen conditions	Young's modulus E (GPa)	Fracture stress σ_f (MPa)	Strain to fracture ε_f (%)	Fracture position
			Thickness in GL t (mm)	Width in GL w (mm)					
Sample A (BW:2138 g, right claw)	Under the fixed finger	CL1	1.94	2.67	wet	17.4	22.7	0.137	within GL
	Under the fixed finger	CL2	1.33	1.97	wet	13.7	46.7	0.340	outside of GL
	Palm	BL1	1.32	2.00	24 h dry	13.5	12.3	0.093	outside of GL
	Palm	BL2	1.35	2.00	wet	–	–	–	'[a]failure
	Palm	BL3	1.54	2.00	wet	12.1	30.0	0.278	outside of GL
	Palm	BT1	1.29	1.85	24 h dry	11.8	20.2	0.169	within GL
	Palm	BT2	1.22	2.00	wet	10.2	26.6	0.276	outside of GL
	Palm	BT3	1.44	1.85	wet	12.0	25.3	0.218	outside of GL
Sample B (BW:2138 g, left claw)	Palm	CL3	1.16	1.94	wet	11.0	25.5	0.244	within GL
	Palm	CL4	1.23	1.90	wet	12.7	50.3	0.433	outside of GL
	Palm	BL4	1.16	1.92	wet	12.7	34.8	0.276	outside of GL
	Palm	BL5	1.42	2.00	24 h dry	12.8	29.9	0.235	within GL
	Palm	BL6	–	–	24 h dry	–	–	–	'*failure
	Palm	BT4	1.43	1.92	wet	13.6	34.6	0.255	outside of GL
	Palm	BT5	1.09	1.90	24 h dry	13.1	35.0	0.270	outside of GL
	Palm	BT6	1.13	1.90	24 h dry	12.8	34.9	0.275	outside of GL
	Under the fixed finger	CL5	1.18	1.98	wet	14.5	37.4	0.264	within GL
Sample C (BW:2038 g, left claw)	Under the fixed finger	CL6	1.18	2.13	wet	12.6	45.7	0.438	within GL
	Under the fixed finger	CL7	1.14	1.96	24 h dry	16.2	31.3	0.200	within GL
	Palm	BL7	1.16	1.99	wet	14.1	27.1	0.195	outside of GL
	Palm	BL8	1.12	1.93	24 h dry	13.9	24.3	0.176	outside of GL
	Palm	BL9	1.13	1.95	24 h dry	12.2	27.2	0.214	outside of GL
	Palm	BT7	1.19	2.05	wet	13.0	32.8	0.261	within GL
	Palm	BT7′	1.08	1.97	wet	15.0	50.5	0.360	within GL
	Palm	BT8	1.11	1.95	24 h dry	14.0	38.1	0.268	outside of GL
	Palm	BT9	1.13	1.94	24 h dry	12.6	35.3	0.280	within GL
					wet	13.2 ± 1.71	35.0 ± 9.4	0.28 ± 0.08	
					dry	13.3 ± 1.17	28.9 ± 7.6	0.22 ± 0.06	
			Mud crab shell [13]		wet	0.48 ± 0.075	30.1 ± 5.0	6.2	
					dry	0.64 ± 0.089	23.0 ± 3.8	3.9	
			Sheep crab leg [10]		wet	0.52 ± 0.075	31.5 ± 5.4	6.4 ± 1.0	
					dry	0.76 ± 0.083	12.9 ± 1.7	1.8 ± 0.3	

[a] failure indicates a specimen broken during installation.

stress, strain to fracture, and fracture position.

Fig. 4 shows contour maps of H_{IT} and E_S obtained from NI testing of the BT9 dray specimen and EDS maps. Representative indentation responses were shown in Fig. S3 of the supplementary material. In addition, for comparison, the $\sigma-\varepsilon$ curve of this specimen is shown in Fig. S4 in the supplementary material. The number of indentations was 920 points on the cross-sectional plane. The distribution of properties was visible (Fig. 4(b and c)), and the regions of high properties corresponded to the streaks with different contrasts seen in the thickness direction on the cross section (Fig. 4(a)). This is associated with local differences in the grade of mineralization in the crab endocuticle material, as shown in Fig. 4(d). For the BT9, the average H_{IT} and E_S—including their standard deviation—were 0.28 ± 0.16 (GPa) and 11.11 ± 3.56 (GPa), respectively. The average E_S was in close agreement with E = 12.6 GPa, as evaluated from the $\sigma-\varepsilon$ curves shown in Fig. 2(f) and S4.

4. Conclusion

In summary, in the endocuticle sample of the mud crab, the fracture stress and the strain to fracture in the wet condition were higher than those for the dry condition. The $\sigma-\varepsilon$ curves of 6 specimens in the wet condition showed nonlinear behavior. However, there were variations

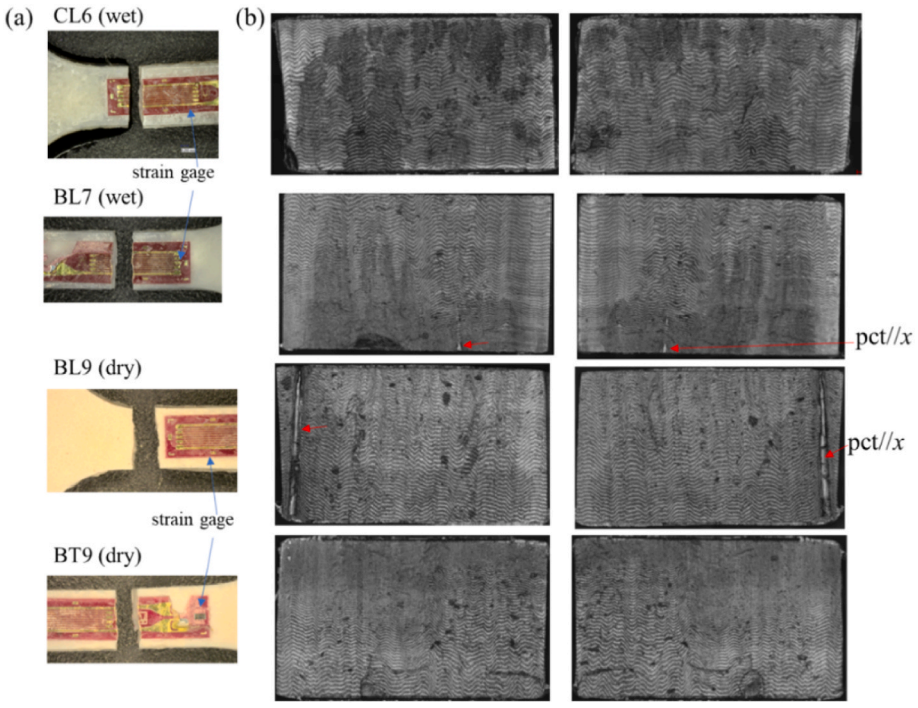

Fig. 3. (a) Appearance of specimens after tensile testing and (b) fracture surfaces.

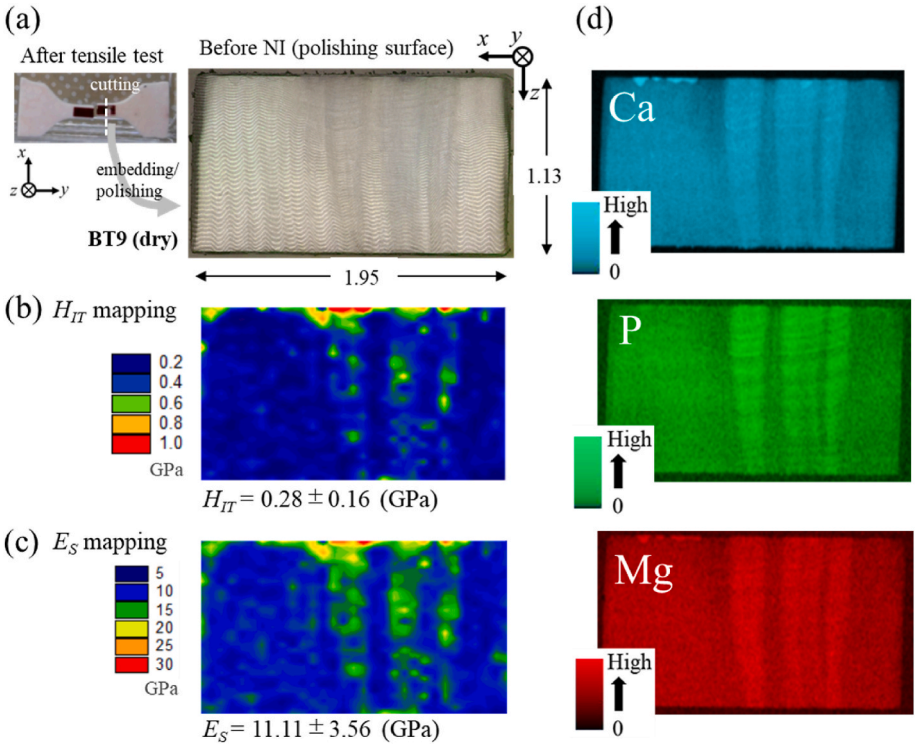

Fig. 4. (a) BT9 dry specimen after tensile testing, polishing surface before nanoindentation testing, and contour maps of (b) hardness, H_{IT}, and (c) Young's modulus, E_S, obtained from nanoindentation testing. Here, the NI test cross section is the position away from the fracture site after tensile testing. (d) EDS maps showing the distribution of calcium (Ca), phosphorus (P), and magnesium (Mg).

in these mechanical properties regardless of whether the specimen condition was dry or wet. This is associated with local differences in the grade of mineralization and the relatively thick pore canal tube penetrating the exoskeleton. The Young's modulus was independent of wet or dry specimen conditions. The average Young's modulus obtained from NI testing performed under the dry condition agreed with the Young's modulus obtained from the $\sigma-\varepsilon$ curve. Since the exoskeletons have local differences in the grade of mineralization, NI testing in extensive regions of the target layer is required to determine exact Young's modulus of its layer.

CRediT authorship contribution statement

Tadanobu Inoue: Conceptualization, Methodology, Software, Validation, Investigation, Resources, Data curation, Writing – original draft, Writing – review & editing, Visualization, Supervision, Project administration, Funding acquisition. **Qiu Hai:** Investigation, Methodology, Data curation, Writing – review & editing. **Koji Nakazato:** Resources, Data curation, Writing – review & editing.

Declaration of competing interest

The authors declare that they have no known competing financial interests or personal relationships that could have appeared to influence the work reported in this paper.

Acknowledgments

We would like to thank Ms. Henmi for preparing the tensile specimens, Ms. Hara and Ms. Sakano for supporting the microstructural observations, and Ms. Kashihara for creating the illustrations. This study was supported by JSPS KAKENHI Grant Number JP21H04537, Japan; Iketani Science and Technology Foundation Grant Number. 0361243-A, Japan. The grants are greatly appreciated.

Appendix A. Supplementary data

Supplementary data to this article can be found online at https://doi.org/10.1016/j.jmrt.2024.09.194.

References

[1] Bai L, Liu L, Esquivel M, Tardy BL, Huan S, Niu X, Liu S, Yang G, Fan Y, Rojas OJ. Nanochitin: chemistry, structure, assembly, and applications. Chem Rev 2022;122:11604–74. https://doi.org/10.1021/acs.chemrev.2c0012.

[2] Naleway SE, Taylor J, Porter MM, Meyers MA, McKittrick J. Structure and mechanical properties of selected protective systems in marine organisms. Mater Sci Eng C 2016;59:1143–67. https://doi.org/10.1016/j.msec.2015.10.033.

[3] Amorim L, Santos A, Nunes JP, Viana JC. Bioinspired approaches for toughening of fibre reinforced polymer composites. Mater. & Design 2021;199:109336. https://doi.org/10.1016/j.matdes.2020.109336.

[4] Yao H, Zheng G, Li W, McDowell MT, Seh Z, Liu N, Lu Z, Cui Y. Crab shells as sustainable templates from nature for nanostructured battery electrodes. Nano Lett 2013;13:3385–90. https://doi.org/10.1021/nl401729r.

[5] Natarajan B, Gilman JW. Bioinspired bouligand cellulose nanocrystal composites: a review of mechanical properties. Phil. Trans. R. Soc. A 2017;376:20170050. https://doi.org/10.1098/rsta.2017.0050.

[6] Wu K, Song Z, Zhang S, Ni Y, Cai S, Gong X, He L, Yu S. Discontinuous fibrous Bouligand architecture enabling formidable fracture resistance with crack orientation insensitivity. Proc Natl Acad Sci USA 2020;117:15465–72. https://doi.org/10.1073/pnas.2000639117.

[7] Inoue T, Hara T, Nakazato K, Oka S. Superior mechanical resistance in the exoskeleton of the coconut crab, *Birgus latro*. Mater Today Bio 2021;12:100132. https://doi.org/10.1016/j.mtbio.2021.100132.

[8] Amini S, Miserez A. Wear and abrasion resistance selection maps of biological materials. Acta Biomater 2013;9:7895–907. https://doi.org/10.1016/j.actbio.2013.04.042.

[9] Sayekti PR, Fahrunnida, Cerniauskas G, Robert C, Retnoaji B, Alam P. The impact behaviour of crab carapaces in relation to morphology. Materials 2020;13:3994. https://doi.org/10.3390/ma13183994.

[10] Chen PY, Lin AY, McKittrick J, Meyers MA. Structure and mechanical properties of crab exoskeletons. Acta Biomater 2008;4:587–96. https://doi.org/10.1016/j.actbio.2007.12.010.

[11] Ma Y, Guo C, Dai N, Shen J, Guan J. Structural characterization and regulation of the mechanical properties of the carapace cuticle in tri-spine horseshoe crab (*Tachypleus tridentatus*). J. Mechanical Behavior of Biomedical Mater 2022;125:104954. https://doi.org/10.1016/j.jmbbm.2021.104954.

[12] Sachs C, Fabritius H, Raabe D. Experimental investigation of the elastic–plastic deformation of mineralized lobster cuticle by digital image correlation. J. Structural Biology 2006;155:409–25. https://doi.org/10.1016/j.jsb.2006.06.004.

[13] Hepburn HR, Joffe I, Green N, Nelson KJ. Mechanical properties of a crab shell. Comp Biochem Physiol 1975;50A:551–4. https://doi.org/10.1016/0300-9629(75)90313-8.

[14] Wang Y, Li X, Li J, Qiu F. Microstructure and mechanical properties of the dactylopodites of the Chinese mitten crab (*Eriocheir sinensis*). Appl Sci 2018;8:674. https://doi.org/10.3390/app8050674.

[15] Raabe D, Sachs C, Romano P. The crustacean exoskeleton as an example of a structurally and mechanically graded biological nanocomposite material. Acta Mater 2005;53:4281–92. https://doi.org/10.1016/j.actamat.2005.05.027.

[16] Shen Z, Su Y, Liang Z, Long X. Review of indentation size effect in crystalline materials: progress, challenges and opportunities. J Mate Res Technol 2024;31:117–32. https://doi.org/10.1016/j.jmrt.2024.06.071.

[17] Long X, Shen Z, Li J, Dong R, Liu M, Su Y, Chen C. Size effect of nickel-based single crystal superalloy revealed by nanoindentation with low strain rates. J Mate Res Technol 2024;29:2437–47. https://doi.org/10.1016/j.jmrt.2024.01.279.

[18] Mirhakimi A, Dubey D, Elbestawi MA. Laser powder bed fusion of bio-inspired metamaterials for energy absorption applications: a review. J Mate Res Technol 2024;31:2126–55. https://doi.org/10.1016/j.jmrt.2024.01.279.

[19] Inoue T, Oka S, Hara T. Three-dimensional microstructure of robust claw of coconut crab, one of the largest terrestrial crustaceans. Mater. & Design 2021;206:109765. https://doi.org/10.1016/j.matdes.2021.109765.

[20] Fabritius H, Karsten ES, Balasundaram K, Hild S, Huemer K, Raabe D. Correlation of structure, composition and local mechanical properties in the dorsal carapace of the edible crab Cancer pagurus. Z.Kristallogr 2012;227:766–76. https://doi.org/10.1524/zkri.2012.1532.

[21] Qiu H, Ueji R, Kimura Y, Inoue T. Heterogeneous distribution of microstrain evolved during tensile deformation of polycrystalline plain low carbon steel. Metals 2020;10:774. https://doi.org/10.3390/met10060774.

[22] Qiu H, Ueji R, Kimura Y, Inoue T. Grain-to-grain interaction effect in polycrystalline plain low-carbon steel within elastic deformation region. Materials 2021;14:1865. https://doi.org/10.3390/ma14081865.

[23] Inoue T, Hiroto T, Hara Y, Nakazato K, Oka S. Tissue structure and mechanical properties of the exoskeleton of the huge claws of the mud crab, *Scylla serrata*. J Mater Sci 2023;58:1099–115. https://doi.org/10.1007/s10853-022-08083-x.

[24] Inoue T, Kitahara E, Hara Y, Nakazato K. Mud crab's mottled, deep blue exoskeleton: surface morphology and internal microstructure. Minerals 2022;12:1607. https://doi.org/10.3390/min12121607.

[25] Oliver WC, Pharr GM. An improved technique for determining hardness and elastic modulus using load and displacement sensing indentation experiments. J Mater Res 1992;7:1564–83. https://doi.org/10.1557/JMR.1992.1564.

[26] Inoue T, Oka S, Nakazato K, Hara T. Structural changes and mechanical resistance of claws and denticles in coconut crabs of different sizes. Biology 2021;10:1304. https://doi.org/10.3390/biology10121304.

[27] Vittori M, Srot V, Korat L, Rejec M, Sedmak P, Bussmann B, Predel F, Aken PA, Štrus J. The Mechanical consequences of the interplay of mineral distribution and organic matrix orientation in the claws of the sea slater *Ligia pallasii*. Minerals 2021;11:1373. https://doi.org/10.3390/min11121373.